Nanochem Res 5(2): 197-210, Summer and Autumn 2020

RESEARCH PAPER

Sunlight Assisted Photodecolorization of Methylene Blue Catalyzed by $H_3PW_{12}O_{40}$ Grafted on APTMS-Graphene Oxide

Bahareh Forghani, Razieh Fazaeli*, Hamid Aliyan

Department of Chemistry, Shahreza Branch, Islamic Azad University, Iran

ARTICLE INFO

Article History:
Received 02 August 2020
Accepted 07 September 2020
Published 15 October 2020

Keywords:
Graphene oxide (GO)
Heterogeneous photocatalysis
Polyoxotungstate
Photodecolorization
Sunlight
Methylene Blue (MB)

ABSTRACT

Surface of graphene oxide was modified by grafting 3-aminopropyl-triethoxysilane to have the positive charge, and thus, to provide sites for the immobilization of $H_3PW_{12}O_{40}$. This modified-nanosized material (PW_{12}-APTMS@GO) was characterized by FTIR, XRD, BET, SEM and TEM. XRD shows that the structure of graphene remains intact after two steps of modifications, while spectral techniques show the successful grafting of PW_{12} on the graphene layers. PW_{12}-APTMS@GO was used as a catalyst in the photodecolorization process of methylene blue dye in aqueous solution under sunlight radiation. The optimum values of the experimental parameters affecting the degradation efficiency were obtained as: 0.015 g L^{-1} of the photocatalyst, 30 ppm dye concentration and pH 3.0. It was found that the catalyst exhibits a significantly high catalytic stability, and the activity loss is negligible after five methylene blue degradation cycles.

How to cite this article
Forghani B, Fazaeli R, Aliyan H. Sunlight Assisted Photodecolorization of Methylene Blue Catalyzed by $H_3PW_{12}O_{40}$ Grafted on APTMS-Graphene Oxide. Nanochem Res, 2020; 5(2):197-210. DOI: 10.22036/ncr.2020.02.010

INTRODUCTION

Recently the photocatalytic mineralization of a great variety of chemicals has been demonstrated using polyoxometalates (POMs), providing an interesting route to the destruction of toxic and hazardous pollutants even in ppb or few ppm levels [1-5]. POMs are acid condensation products, mainly of molybdenum and tungsten [6,7] that become powerful oxidizing reagents upon excitation with near-visible and UV light, capable of destroying a great variety of pollutants in the aquatic environment [1-8].

Infact, many of POMs share very similar ohotochemical characteristics of the semiconductor photocatalysts, and POMs represent the analogues of semiconductor metal oxides [9-13]. That is, both classes of materials are constituted by a d^0 transition metal and oxide ions and exhibit similar electronic attributes including well-defined HOMO-LUMO gaps (semiconductor "band gaps"). The "gaps" inhibit the recombination of electrons and holes that are generated by the irradiation of the surface of the photocatalysts with the light energy higher than or equal to their band gap energy. These photogenerated electrons and holes thus are capable of initiating the chemical reaction due to the strong photooxidative ability of the holes and photoreductive ability of the electrons.

In most of the proposed mechanisms concerning the photocatalytic degradation of organic pollutants (S), in the presence of POM, the oxidation is supposed to be performed by highly oxidizing ×OH radicals produced indirectly [14], through the reaction of excited POM (POM*) with water. The overall reactions taking place in a photocatalytic circle in the presence of oxygen are as follows (Eqs. 1-4):

$$POM + h\nu \rightarrow POM^* \qquad \text{i.e. } POM\ (h^+ + e^-) \qquad (1)$$

* Corresponding Author Email: *fazaeli@iaush.ac.ir*

$$POM(h^+ + e^-) + H_2O \rightarrow POM(e^-) + {}^{\times}OH + H^+ \quad (2)$$

$${}^{\times}OH + S \rightarrow \text{oxidation products} \rightarrow\rightarrow\rightarrow CO_2, H_2O \text{ and inorganic ions} \quad (3)$$

$$POM\ (h^+ + e^-) + S \rightarrow POM\ (e^-) + S^+ \rightarrow\rightarrow\rightarrow CO_2, H_2O \text{ and inorganic ions} \quad (4)$$

Dioxygen is a very effective oxidant for the reduced POM [15-17], thus its main action is the regeneration of the catalyst (Eq. 5):

$$POM\ (e\text{-}) + O_2 \rightarrow POM + O_2^- \quad (5)$$

This superoxide radical anion O_2^- ($H^+ + O_2^- \rightarrow HO_2^{\times}$ pka = 4.8) [18] may participate further in oxidative processes (Eq. 6) [18]:

$$O_2^-/HO_2 + S \rightarrow \text{oxidation products} \quad (6)$$

as well as reductive processes [19].

Thus, upon photolysis of an aqueous solution of POM both oxidative and reductive species are formed. The oxidative species are ×OH radicals, the excited POM and the superoxide radical anions, while the reductive species are reduced POM, POM(e^-), and the superoxide radical anions.

Graphene –a single-atom-thick sheet consisting of sp^2 hybridized carbon atoms is the building block of all graphitic carbons. Graphene has attracted tremendous interest due to its unique properties including high electronic conductivity, high modulus, and high surface area. These unique properties have led to numerous applications in both electronic devices [20] and composite materials [21]. Moreover, with both high surface area and high chemical stability, graphene can be used as a gas adsorbent [22], as the active material for ultracapacitors [23], or as a support for heterogeneous catalysts [24]. Grapheneoxide (GO) is one of the fascinating host materials. GO-based materials are oth the perspective of fundamental science and technology, because they are nontoxic, chemically tolerant and mechanically hard. Such properties suggest wide application of GO-based materials, such as catalyst supports, structural components, and energy storage.

In continuation of our work on the catalytic properties of heteropoly acids (HPAs) [25-28], the focus of the present work is on the synthesis of PW_{12}-APTMS@GO and its use in the photodecolorization of methylene blue (MB); (C.I.No: 52015, formula weight (anhydrous basis) = 319.85, structure shown in Fig. 1), using sunlight irradiation. The rate determining parameters like initial dye concentration, catalyst loading, pH of the medium, temperature of the dye solution on the photodecolorization of MB are studied in detail.

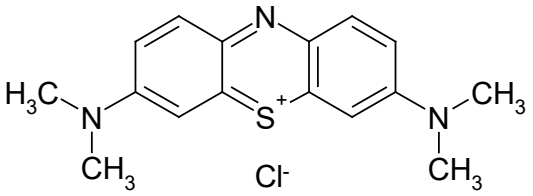

Fig. 1. Molecular structure scheme of the methylene blue.

EXPERIMENTAL

All materials were commercial reagent grade. Infrared spectra (400–4000 cm^{-1}) were recorded from KBr pellets on a PerkinElmer Spectrum 65 spectrometer. The X-ray powdered diffraction patterns were performed on a Bruker-D8ADVANCE with automatic control. The patterns were run with monochromatic Cu Kα (1.5406 Å) radiation with a scan rate of 2^o min^{-1}. Nitrogen adsorption measurements were performed at −196◦C by using an ASAP 2010M surface analyzer, and the pretreatment temperature was 180◦C. Transmission electron micrographs (TEM) were obtained on a Joel JEM 2010 scan-transmission electron microscope. The sample for the TEM measurement was suspended in ethanol and supported on a carbon coated copper grid.

Synthesis of grapheme oxide (GO)

Some modifications were made to the Hummers method [29] and applied to the preparation of GO from industrially expanded graphite (Scheme 1). In a typical reaction, potassium permanganate (15 g) and expanded graphite (5 g) were initially stirred until the mixture became homogeneous. Then, in a bottom-round flask (500 mL) with ice-water bath, concentrated sulfuric acid (98 %, 100 mL) was added to the mixture while stirring continuously until a uniform liquid paste was formed. Then, the water bath was removed. The stirring continued until a foam-like intermediate spontaneously formed (around 30 min) at room temperature with a large volumetric expansion. Deionized water (400 mL) was added, and rapid stirring was restarted to prevent effervescing. Next, the flask was placed in

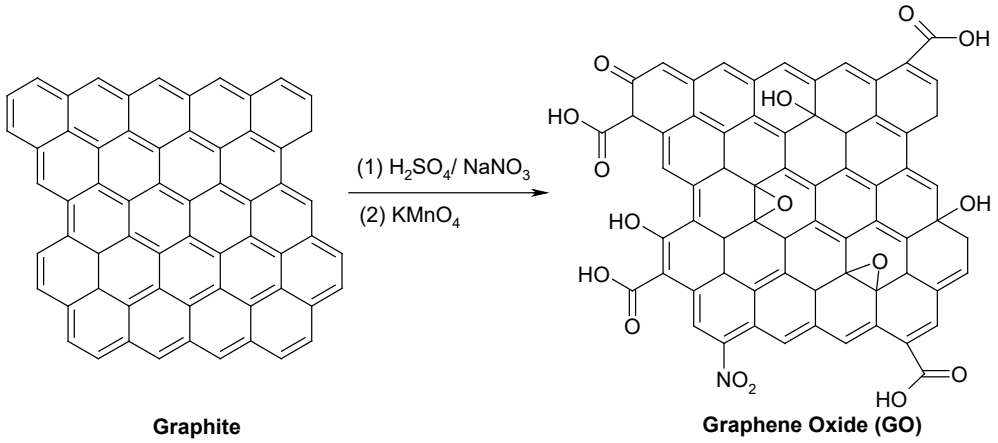

Scheme 1. Synthesis of GO.

a 90°C water bath, and after 1 h a homogeneous suspension was obtained that was dark yellow in color. The suspension was then filtered and was subjected to repeated washing and centrifugation (10000 rpm, 2 h per cycle) to remove impurities. To fully exfoliate the GO sheets, the resulting solution was sonicated using a tabletop ultrasonication cleaner (100 W).

Surface modification of GO and immobilization of $H_3PW_{12}O_{40}$ (PW_{12})

Scheme 1 shows the procedures for the surface modification of GO samples and the subsequent immobilization of $H_3PW_{12}O_{40}$ (PW_{12}) on the surface modified GO (APTMS@GO). Surface modification of GO was done by a grafting method (Scheme 2).

To a suspension of 10 g of GO in 50 ml dry

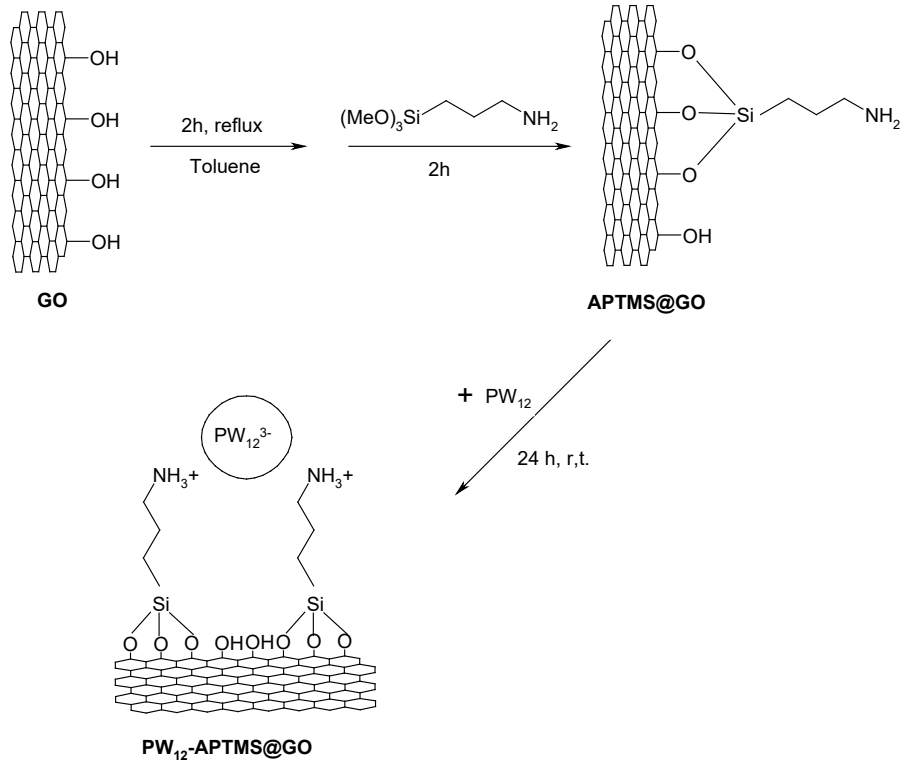

Scheme 2. The procedures for the surface modification of GO and the subsequent immobilization of PW_{12} on the surface modified GO.

toluene, 2.68 g of 3-aminopropyl triemethoxy silane (APTMS) was added slowly and heated to reflux with continuous stirring for 8 h under nitrogen atmospheres. The powder sample containing amino groups was filtered, washed with acetone and then soxhlet was extracted using a solution mixture of diethyl ether and dichloromethane (1:1) for 24 h and dried under vacuum. It was finally calcined at 180◦C for 2 h to yield the APTMS@GO. Immobilization of PW_{12} on the APTMS@GO was achieved as following: APTMS@GO (1.0 g) was added into the acetonitrile solution containing 0.5 g of PW_{12} with vigorous stirring at room temperature, and the resulting solution was maintained at room temperature for 24 h. The solid product was filtered, and then it was dried overnight at 80◦C to yield the PW_{12}-APTMS@GO.

The catalytic activity

The photodecolorization experiments were carried out with sunlight under clear sky in summer (June–August). The intensity of sunlight was measured about 296 Wm^{-2} s^{-1}, using Daystar solar meter (USA). A certain amount of the photocatalyst was suspended in 10 mL of 20 ppm MB solution in a closed wide cylindrical glass vessel with an appropriate height. Photometric analysis of samples before and after of irradiation can be used for the measurement of decolorization efficiency of dye (%D). The absorbance of samples was measured by a UV–Vis spectrophotometer, Carry 100 Scan, using a paired 1.0 cm quartz cell. The concentration change was calculated from the linear calibration plot of MB at a wavelength of 665 nm. The decolorization efficiency of the dye was determined by the following equation (Eq. 7):

$$Decolorization\ \% = \frac{C_0 - C}{C_0} \times 100 \quad (7)$$

which C_o is the initial concentration of dye and C is the concentration of dye after irradiation in a specified time interval. In order to obtain maximum decolorization efficiency, the effects of key operating parameters such as dosage of photocatalyst (0.009–0.02 g L^{-1}), initial concentration of MB (10-30 ppm) and solution pH (3–11) on photodecolorization process were studied. To investigate the extent of surface adsorption during the decolorization of MB, control experiments in dark condition were performed at the presence of catalysts, in accordance to each case.

The decolorization of MB dye fitted with first order kinetics [ln (C/C°)=−kt] (where C° and C are the dye concentration in the absence and presence of the photocatalyst under UV irradiation, respectively, and k (min^{-1}) is the reaction rate constant). The rate constant, k, was calculated from the slopes of the straight-line portion of the plots of ln (C/C°) vs. time. To determine the surface adsorption amounts, control experiments in dark conditions were carried out in the presence of catalyst in solutions of MB.

RESULTS AND DISCUSSION

Physico-chemical characterization

FT-IR spectra of GO, PW_{12} and PW_{12}-APTMS@GO in the skeletal region of 4000–400 cm^{-1} are shown in Fig. 2. The primary structure of bulk PW_{12} could be identified by four characteristic IR bands appearing at 1080 cm^{-1} (P-O band), 990 cm^{-1} (W=O band), 890 and 810 cm^{-1} (W-O-W bands) (Fig. 2a). FT-IR spectrum of the graphene oxide obtained confirms the successful oxidation of the graphite as shown in Fig. 2b. The presence of different types of oxygen functionalities in graphene oxide was confirmed by a broad, wide

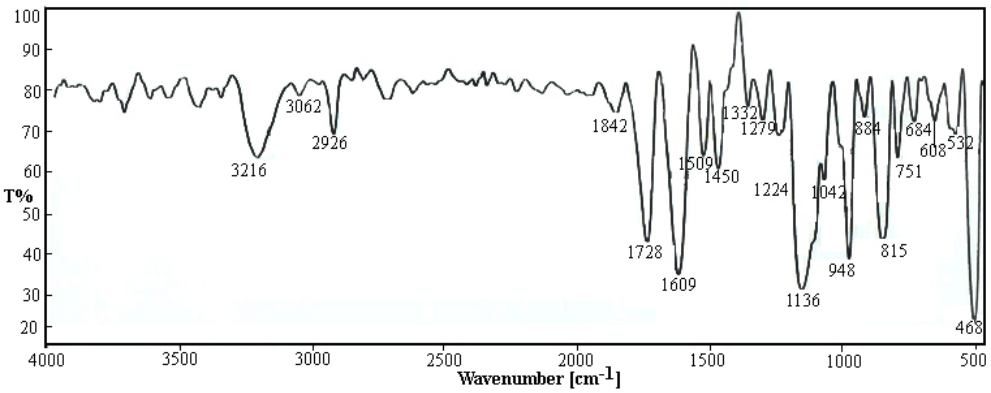

Fig. 2. FTIR spectra of PW_{12}-APTMS@GO.

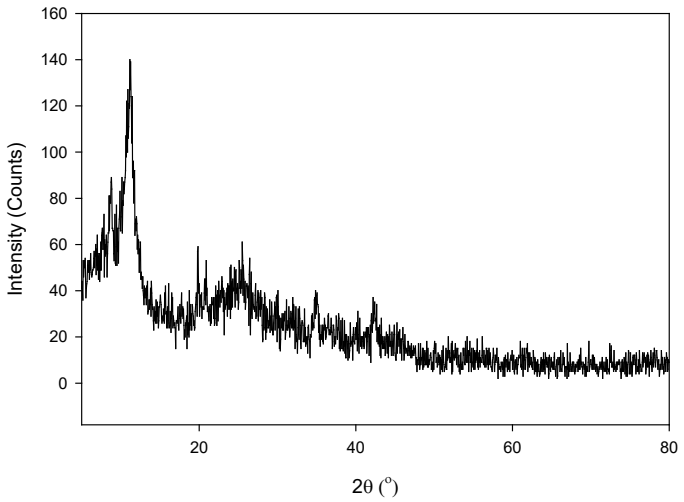

Fig. 3. XRD patterns of PW_{12}-APTMS@GO.

peak at 3447 cm^{-1} which can be attributed to the O-H stretching vibrations of the C-OH groups and water [30, 31]. The absorption bands at 1560 cm^{-1} can be ascribed to benzene rings [32]. The sharp intense peak at 1419 cm^{-1} can be attributed to CO carboxylic group. FT-IR is known as a powerful technique for the study of surface interaction between heteropolyacid and organic and inorganic supports. The FTIR spectrum of PW_{12}-APTMS@GO (Fig. 2c) shows four bands in the range of 1250–500 cm^{-1}. It was found that for 110°C dried samples the Keggin bands are observed at 1097, 947, 890 and 810 cm^{-1} for PW_{12}-APTMS@GO.

The XRD pattern of PW_{12}@GO is shown in Fig. 3. The XRD patterns of GO show a diffraction peak around 12.31 [29]. The peak positions in the XRD pattern of PW_{12}-APTMS@GO composite materials are not changed after PW_{12} incorporation and are in a good agreement with its parent GO.

Figs. 4a-4f show the scanning electron microscopy (SEM) image of the PW_{12}-APTMS@GO material. The PW_{12}-APTMS@GO exhibits much rougher surfaces than the aggregated graphene nanosheets in a dried state reported by Samulski et al., [24] which might be attributed to the adsorption of PW_{12} nanoparticles on the surface of graphene sheets, and the electrical density of PW_{12} nanoparticles is different from that of graphene sheets.

The TEM images of PW_{12}-APTMS@GO sample are shown in Figs. 4g-4j. The synthesized GO clearly displayed layered structure [32]. The same morphology obtained for PW_{12}-APTMS@GO.TEM analyses indicate that the structure of the GO is robust enough to survive the PW_{12} incorporation process and so offers an excellent matrix to support highly dispersed PW_{12} species. The places with darker contrast could be assigned to the presence of PW_{12} particles with different dispersions.

Fig. 5 shows the N_2 adsorption–desorption isotherms and pore size distributions of PW_{12}-APTMS@GO composite. The sample exhibited typical IV type isotherm and H1 type hysteresis loops at high relative pressures. PW_{12}-APTMS@GO showed BET surface area of 55.8 m^2/g.

Evaluation of photocatalytic activity of PW_{12}-APTMS@GO

Effect of the amount of catalyst

The effect of the amount of PW_{12}-APTMS@GO on the photocatalytic decolorization of the MB was studied in the range of 0.009-0.02 g L^{-1} and the obtained results are presented in Fig. 6. The rate constant values, k (min^{-1}), were also calculated from the straight-line segment of the corresponding first-order plots as a function of the catalyst mass and the results are listed in Table 1. The dye decolorization increased with increasing the catalyst concentration. By increasing the amount of catalyst, the number of active sites on the photocatalyst surface increases and also causes an increase in the number of $OH^{\cdot}$ radicals which can take part in the decolorization of the dye in solution [33,34]. It was found that the decolorization rate decreases with further increase in the catalyst concentration because of the light

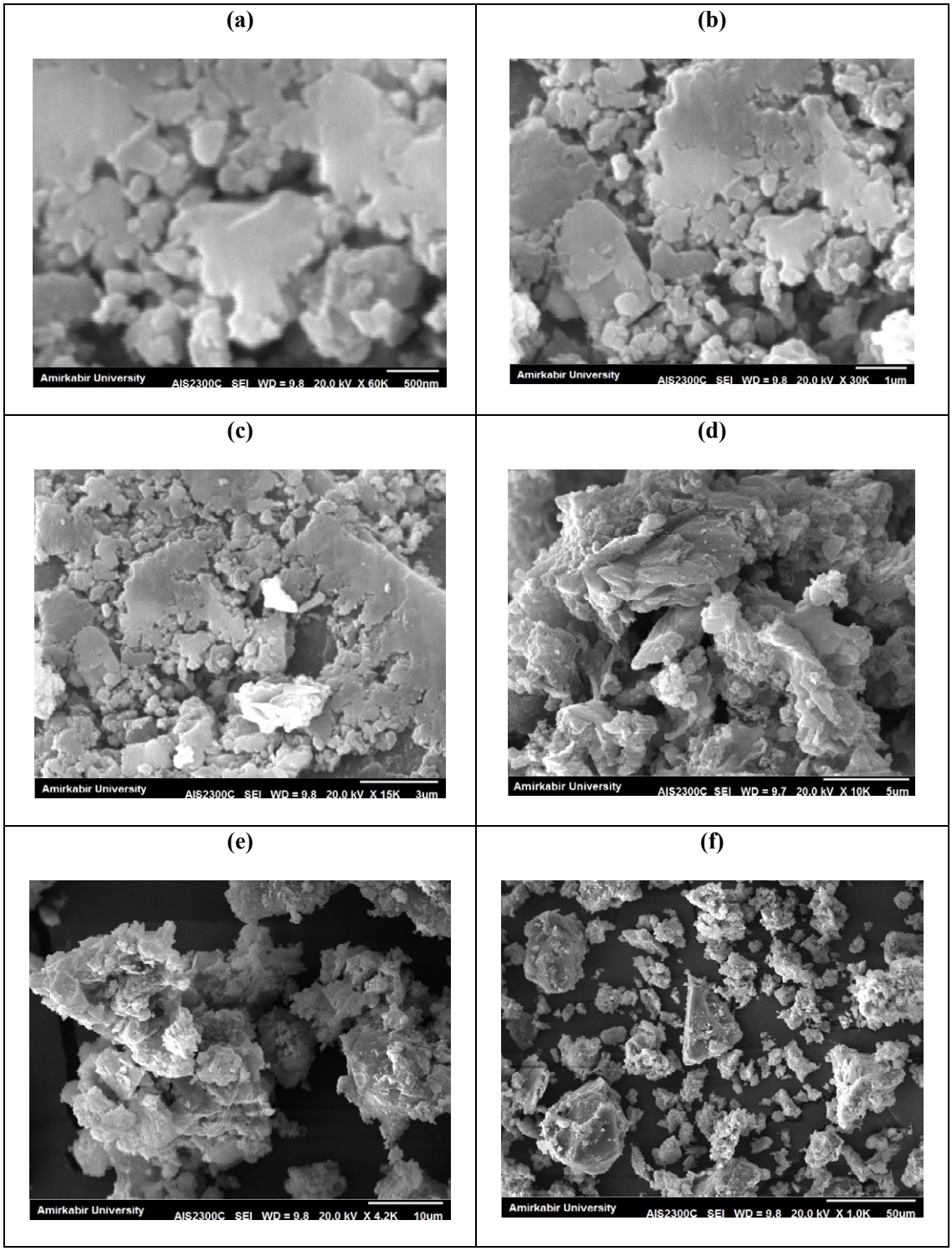

Fig. 4. (a-f) SEM and (g-j) TEM images of PW_{12}-APTMS@GO samples.

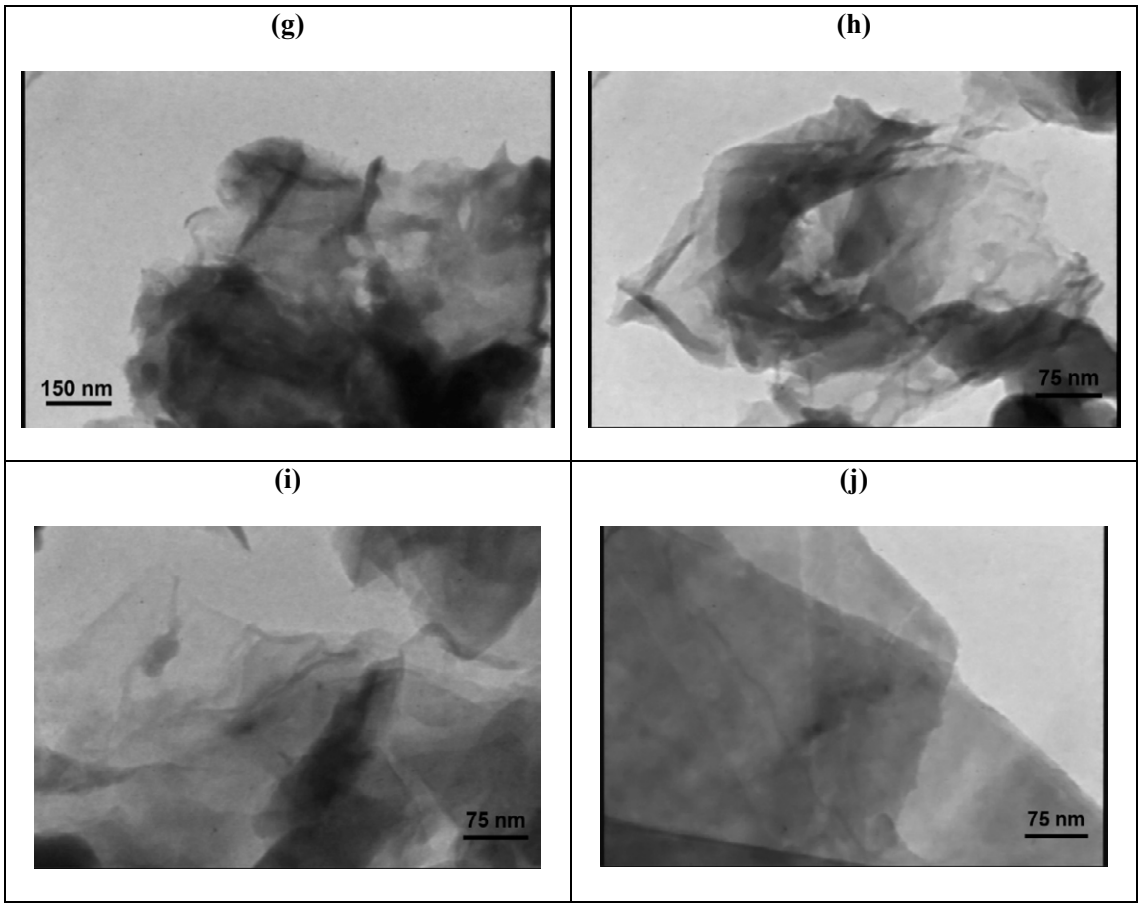

Continued Fig. 4. (a-f) SEM and (g-j) TEM images of PW_{12}-APTMS@GO samples.

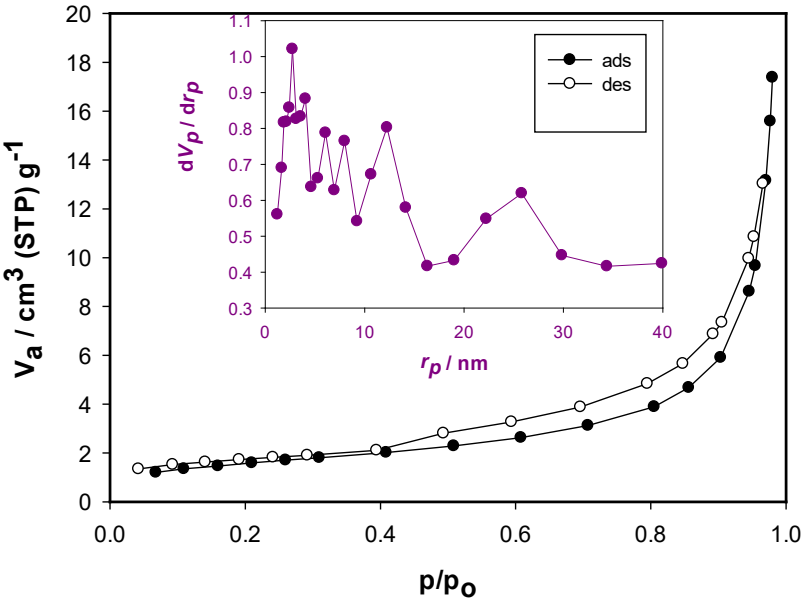

Fig. 5. (a) Effect of the dosage on the degradation efficiency; initial MB concentration, 20 ppm, initial pH, 5; (b) Plot of ln C/C° vs time as a function of catalyst mass.

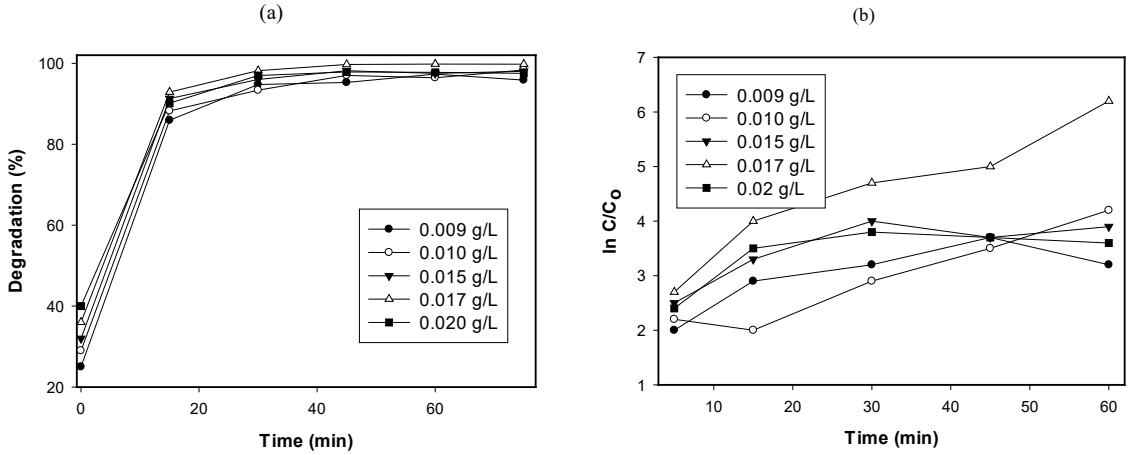

Fig. 6. (a) Effect of the dosage on the degradation efficiency; initial MB concentration, 20 ppm, initial pH, 5; (b) Plot of ln C/C^o vs time as a function of catalyst mass.

Table 1. Reaction rate constant values of MB decolorization as a function of experimental parameters.

Parameter	Value	k ($\times 10^3$ min^{-1})
	0.020	20.4
	0.017	36.7
Catalyst mass (g L^{-1})	0.015	22.9
	0.010	53.1
	0.009	20.8
	10	12.9
	15	10.7
C in mixture of dyes (mgL^{-1})	20	83.0
	25	80.8
	30	88.2
	3	11.8
	5	11.6
pH of solution	7	6.3
	9	11.2
	11	9.5
	40	90.1
Temperature (°C)	60	98.3
	80	105.6

scattering and screening effects [35]. Thus, it can be concluded that the higher loading of the catalyst may not be useful both in view of the aggregation and the reduced irradiation field due to the light scattering phenomena [36]. As expected, the initial rates of degradation increased with increasing in the weight of the catalyst up to an optimum loading of PW_{12}-APTMS@GO (0.010 g L^{-1}) and further increasing had a negative effect.

Effect of the initial MB concentration

Many researchers have studied the effect of the initial concentration of pollutants in the photocatalysis. In all cases, it was found that an increase in the concentration of the contaminant results in a decrease in the photocatalytic reaction rate [37]. Generally, the kinetic follows a Langmuir–Hinshelwood mechanism confirming the heterogeneous catalytic character (Eq. 8) [38],

$$r = \frac{-dc}{dt} = \frac{-kKC_0}{(1+KC_o)} or\ r^{-1} = \left(\frac{1}{kK}\right)C_0^{-1} + \frac{1}{k} \quad (8)$$

where C_o is the initial dye concentration in (mgL^{-1}), c is the concentration of dye solution at any time, r is the reaction rate in (mgL^{-1} min), *k* is the rate constant of photocatalysis in (mgL^{-1} min), K is the rate constant of adsorption in (Lmg^{-1}) (Langmuir constant related to the energy of adsorption) and t

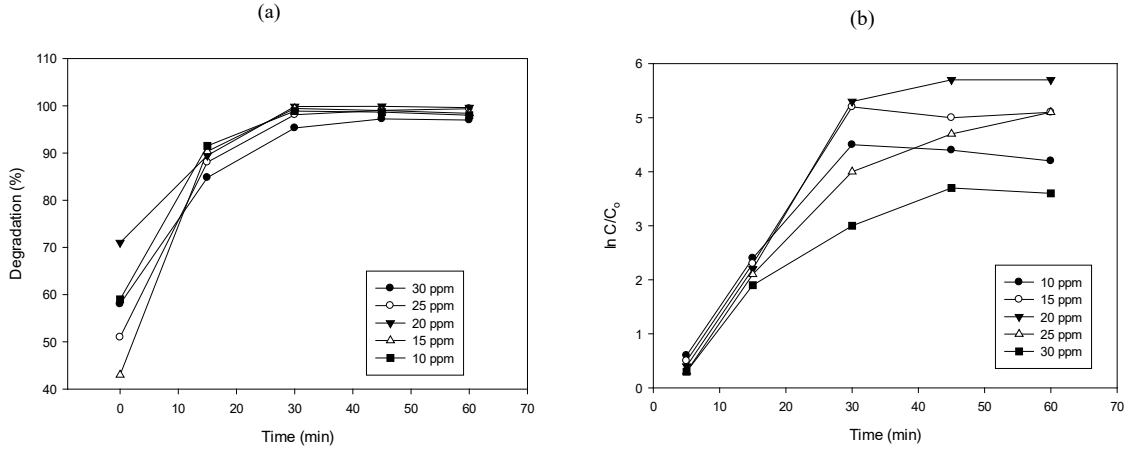

Fig. 7. (a) Effect of initial MB concentration on the degradation efficiency; 0.010 gL^{-1} of the catalyst, initial solution pH, 3; (b) Plot of ln C/C^o vs time as a function of initial concentration.

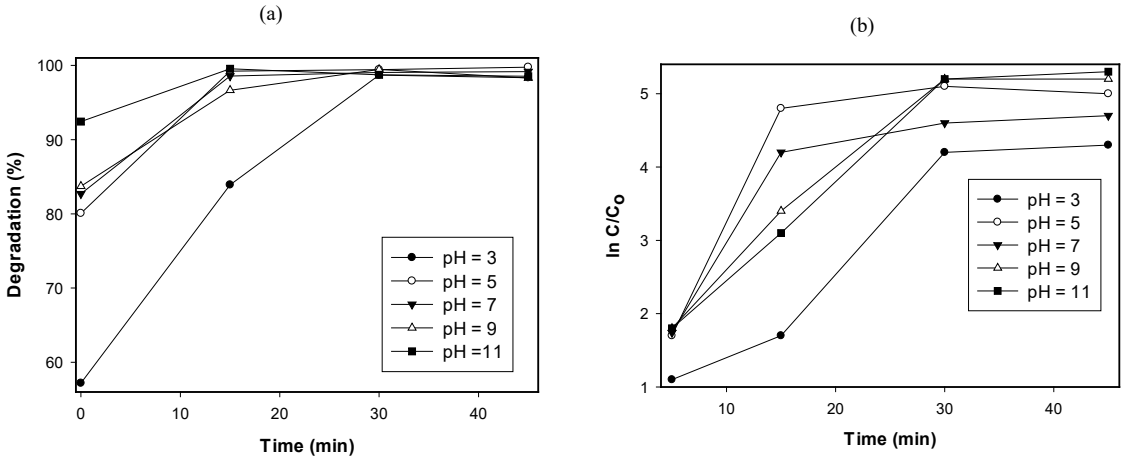

Fig. 8. (a) Effect of solution pH on the degradation efficiency of MB; 0.010g L^{-1} of the catalyst; Initial MB concentration, 30 mgL^{-1}; (b) Plot of ln C/C^o vs time as a function of pH of solution.

in the time in min. For the diluted solutions (< 1.0 mM), KC_0<< 1 because of the weak adsorption of dye on the surface of the catalyst, the above model can be expressed as Eq. (9 or 10):

$$r_0 = kKC_0 = k_1C \quad (9)$$

$\ln C_t/C_o = -k_1t$ (where k_1 is a first-order rate constant in (min^{-1}) (10)

Therefore, the reaction of photocatalytic degradation of dye by the catalyst is an apparent first-order reaction in Langmuir–Hinshelwood model, whose apparent relationships are due to the low concentration of the dye chosen. At low concentrations, the number of catalytic sites will not be a limiting factor and the rate of decolorization is proportional to the concentration of dye [37, 39].

The photocatalytic degradation of MB was investigated at different initial concentrations covering the range from 10 to 50 ppm and the results are collected graphically in Figs. 8, and 9. With increasing the initial concentration, a bigger quantity of MB molecules was adsorbed on the surface of the PW_{12}-APTMS@GO catalyst, and therefore, the generation of hydroxyl radicals would be reduced since there were fewer active sites for the adsorption of hydroxyl ions. Further, at higher

concentration of MB in the solution, the photons would be able to be absorbed by the MB molecules before they could reach the catalyst surface. This in turn reduces the absorption of photons by the catalyst and consequently the degradation efficiency [40]. In addition, the lifetimes of hydroxyl radicals are very short about a few nanoseconds and thus they can only react where they are formed. Increasing the quantity of MB molecules per volume unit logically enhances the probability of collision between organic molecules and oxidizing species, leading to an increase in the degradation efficiency [40,41]. Accordingly, it is important to select an optimum concentration to reach the maximum photodecolorization efficiency. It has been observed that the rate of photodecolorization increases with increasing in dye concentration up to 30 ppm (Fig. 7). This may be due to the fact that by increasing the dye concentration, more dye molecules are available for consecutive degradation. The rate of photodecolorization was found to decrease with further increase in dye concentration; i.e., above 30 ppm. The reason for this decrease is attributed to shielding effect of dye at high concentration that retards the penetration of light to the dye molecules deposited over catalyst surface.

Effect of the solution pH

The effect of solution pH in the range of 3–11 and in the experimental conditions (0.015 g L^{-1} of catalyst, 20 ppm dye) on the overall rate of decolorization was studied. Fig. 8 shows the effect of pH of solutions adjusted before starting photodecolorization on the rate of reactions. The pHs may change during the reactions. As shown in Fig. 8, the maximum decolorization efficiency was obtained in pH=5. This is due the fact that in acidic pH values, associated with HCl acidification of the solution, a high amount of conjugated base is added to the mixture. Chloride anions can react with hydroxyl radicals and produce ClO^- ions which are not as reactive as •OHs; thus, refusing to take part in the dye decolorization process [42]. On the other hand, higher pH results in higher number of hydroxyl ions, and it consequently leads to a higher concentration of hydroxyl radicals participating in the photocatalysis reaction. However, when the pH value is so high (pH=3), there is an abundant number of hydroxyl ions around catalyst competing with dye molecules in adsorption on the surface of photocatalyst; this causes a decrease in photodecolorization efficiency [42,43]. Table 1 shows the rate constant values, k (min^{-1}), as a function of the pH of MB solutions. The obtained

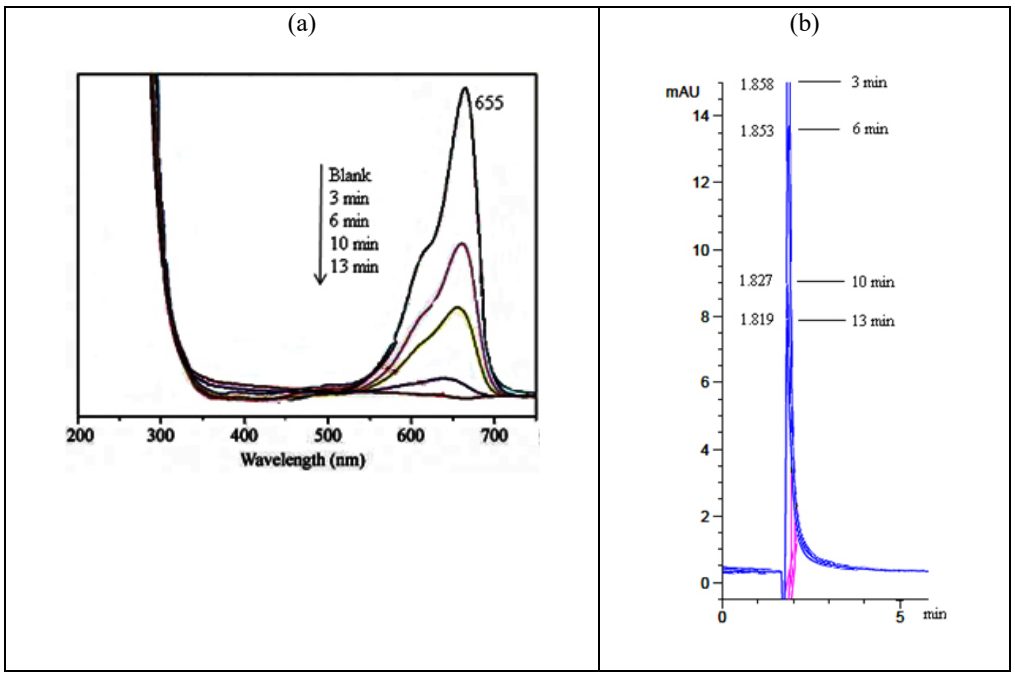

Fig. 9. (a) absorbance spectra of MB at λmax (566) during the course of photodecolorization reaction with optimum conditions. (b) HPLC chromatogram of MB (20 ppm MB solution, pH=3.0) after decolorization process of the sample under sunlight irradiation in the presence of PW_{12}-APTMS@GO photocatalyst (0.01 gL^{-1}) in time interval of 120 min.

results revealed a decrease in removal efficiency at a pH higher than 5 during the decolorization of MB by PW_{12}-APTMS@GO. This suggests that at a high −OH concentration, two processes may take place leading to the deactivation of •OH. First, the $H_2O^{\bullet}_2$ and $HO^{\bullet}_2$ radicals are allegedly formed due to the reaction of •OH with −OH. The reactivity of these radicals with organic dye is very low compared to that of •OH. Second, due to the presence of high amounts of OH radicals, the radical–radical reactions takes place at higher pH values [44]. Although in pH 5 photodecolorization of MB is performed in its highest rate, we did not control the pH of the solutions during the experiments and only the initial pH of solution was adjusted at 5.

Effect of temperature

The photodecolorization of MB was studied at temperature ranging from 35 to 75 °C and experimental conditions (0.015 g L^{-1} of catalyst, 20 ppm dye). The rate constant values, k (min^{-1}), as a function of temperature are listed in Table 1. As shown in Table 1, by increasing the temperature, the decolorization efficiency is increased as well. An increase in temperature helps the reaction to compete more effectively with $e^-_{CB}.h^+_{VB}$ recombination [45-47]. On the other hand, an increase in temperature decreases the solubility of oxygen in water, which is not desirable. Higher temperatures will also cause significant evaporation of the solution during the experiments. Thus, temperatures higher than 50°C are not recommended.

Reusing of supported photocatalyst

Reusability of the catalyst for the degradation of MB was also evaluated. The suspension was centrifuged and the solid material was washed and dried at 100 and 200°C. The dried catalysts were used for the degradation of MB, employing similar experimental conditions. The decreases in the degradation extent after five runs were about 2, 5, 9, 15 and 20% for the reused catalyst at drying temperature of 100°C, while these values were 2, 3.5, 6, 10 and 14% for the reused catalyst at drying temperature of 200°C. The decrease in the degradation extent is explained by adsorption of organic intermediates and by-products of the photodecolorization process in the cavities and on the surface of the photocatalyst that influences the surface activity of the catalyst [48]. Hence, for the dried catalyst at 200°C, decrease in the degradation efficiency is lower than the other cases. On the other hand, at higher temperatures, the excess of adsorbed molecules on the surface was removed and more degradation centers were released. The decrease in the degradation rate was also explained by the ZnO loss from the support surfaces [49]. The heat treatment will also induce the catalyst aggregation after several recycles resulting in the decrease of surface area, finally leading to the decrease in the photocatalytic efficiency. Also, in both cases, the leached zinc cations into the solution decreases the semiconductor as the active sites on the catalyst surface. This in turn reduces the photo-reactivity of the remained catalyst. In addition, in repetitive uses of the catalyst, a loss occurred in the amount of the reused catalyst particles. Hence, it decreases the degradation efficiency in the later runs.

Decolorization pathway

Changwen Hu et al. have reported that both $OH^{\bullet}$ radicals and [POM/SiO_2] are responsible for degradation and mineralization of aqueous malic acid; MA [50]. First, POMs and TiO_2 have the similar structural (both of them have d^0 transition metals and oxide ions) and redox characteristics (excited state redox potential are 2.62V for TiO_2 and 2.63V for POM, respectively), so, there is the possibility for generation of $OH^{\bullet}$ radicals by [POM/SiO_2]. This can be described by Eqs. (11) and (12):

$$POM/SiO_2 + h\nu \rightarrow [POM/SiO_2]^* \text{ or } POM/SiO_2 + h\nu \rightarrow POM/SiO_2(e^- + h^+) \quad (11)$$

$$POM/SiO_2(e^- + h^+) + H_2O \rightarrow POM/SiO_2(e^-) + OH^{\bullet} + H^+ \quad (12)$$

Second, [POM/SiO_2] is a strong photooxidant possessing the ability to undergo a reversible multielectron reduction. Therefore, direct photo-oxidation of an aqueous MA on the surface and in the micropores of the powdered $POMs/SiO_2$ by electron transfer or hydrogen atom abstraction may be also an important mechanistic pathway. Direct oxidation can be described by Eq. (13):

$$[POM/SiO_2]^* + MA \rightarrow [POM/SiO_2]_{red} + MA_{ox} \quad (13)$$

where $[POM/SiO_2]_{red}$ refers to HPB on the surface or in the pores of the catalysts, and MA_{ox} refers to all kinds of the intermediates or final products of MA. We proposed similar mechanism for photodecolorization of MB in the presence of PW_{12}-APTMS@GO.

UV–Vis studies

Fig. 9a shows the photodecolorization of MB under irradiation in the time interval of 50 min and in the presence of PW_{12}-APTMS@GO photocatalyst at the optimum conditions (photocatalyst: 0.0.15 g L^{-1}, dye concentration: 20 ppm and pH= 5). The decrease of samples absorbance due to the decrease of dye concentration was recorded for the measurement of photodecolorization rate in all above-mentioned parameters. Since there were no additional peaks appearing in the UV–Vis spectra the dye was completely degraded.

The extent of degradation and mineralization was also followed using HPLC (Fig. 9b). The HPLC chromatograms show the degradation of pollutant into smaller fragments, which are subsequently mineralized completely. A sharp peak of the dye was detected at 0 h irradiation whereas only 1.82% was observed at the end of 13 min. The dye peak showed a significant decrease at the end of 13 min and some new peaks were observed at different retention times during irradiation confirming the formation of degradation products.

In our experiments, the stability and reusability of the photocatalyst were examined by repetitive use of the catalyst. After the dye was degraded in the first cycle, the photocatalyst was filtered and washed with CH_2Cl_2 and dried at 200°C for 2 h, and then was added again into the same concentration of MB solution. The decomposition of MB in the second cycle was almost as fast as in the first run. Repeatedly, the fifth runs of the degradation of MB showed no significant loss of activity of the catalyst, indicating the considerable stability of the catalyst under the present conditions.

The photocatalytic decolorization reactions of MB can be written as follows [51]:

$$PW_{12}\text{-APTMS@GO /MB} + h \rightarrow PW_{12}\text{-APTMS@GO / MB}^{*} \quad (14)$$

$$PW_{12}\text{-APTMS@GO /MB}^{*} \rightarrow PW_{12}\text{-APTMS@GO } (e_{CB}^{-}) \text{ /MB}^{+} \quad (15)$$

$$PW_{12}\text{-APTMS@GO } (e_{CB}) + O_2 \rightarrow PW_{12}\text{-APTMS@GO} + \cdot O_2^{-} \quad (16)$$

$$\cdot O_2^{-} + H^{+} \rightarrow HOO\cdot \rightarrow \cdot OH \quad (17)$$

$$h_{VB}^{+} + OH^{-} \rightarrow \cdot OH \quad (18)$$

$$\cdot OH + MB \rightarrow \text{degradation products} \quad (19)$$

CONCLUSION

The results of this research demonstrated that PW_{12}-APTMS@GO can perform as a catalyst affecting on the photodegredation of MB using sunlight as a radiation source. Applying a small amount of catalyst, spending a short time for completing the decolorization process (>98% of photodecolorization in about 20 min), and utilizing sunlight as the radiation source are the advantages of our proposed method, which in turn results in less environmental contamination and saves time and energy. The results of UV–Vis spectra changes and HPLC methods indicate that photocatalytic process can be used for the complete decolorization and mineralization of the pollutant in a photochemical reactor.

ACKNOWLEDGEMENTS

We gratefully thank Shahreza Branch, Islamic Azad University, for financial support.

CONFLICT OF INTEREST

The authors confirm that this article content has no conflict of interest.

REFERENCES

1. Hiskia A, Mylonas A, Tsipi D, Papaconstantinou E. Photocatalytic Degradation of Lindane in Aqueous Solution. Pesticide Science. 1997;50(2):171-4.
2. Mylonas A, Hiskia A, Papaconstantinou E. Contribution to water purification using polyoxometalates. Aromatic derivatives, chloroacetic acids. Journal of Molecular Catalysis A: Chemical. 1996;114(1-3):191-200.
3. Hiskia A, Androulaki E, Mylonas A, Boyatzis S, Dimoticali D, Minero C, et al. Photocatalytic mineralization of chlorinated organic pollutants in water by polyoxometallates. Determination of intermediates and final degradation products. Research on Chemical Intermediates. 2000;26(3):235-51.
4. Texier I, Giannotti C, Malato S, Richter C, Delaire J. Solar photodegradation of pesticides in water by sodium decatungstate. Catalysis Today. 1999;54(2-3):297-307.
5. Hu C, Yue B, Yamase T. Photoassisted dehalogenation of organo-chlorine compounds by paratungstate A in aqueous solutions. Applied Catalysis A: General. 2000;194-195:99-107.
6. Pope MT, Müller A. Polyoxometalate Chemistry: An Old Field with New Dimensions in Several Disciplines. Angewandte Chemie International Edition in English. 1991;30(1):34-48.
7. Day VW, Klemperer WG. Metal Oxide Chemistry in Solution: The Early Transition Metal Polyoxoanions. Science. 1985;228(4699):533-41.
8. Gu C, Shannon C. Investigation of the photocatalytic activity of TiO2–polyoxometalate systems for the oxidation of methanol. Journal of Molecular Catalysis A: Chemical. 2007;262(1-2):185-9.

9. Proust A, Thouvenot R, Gouzerh P. Functionalization of polyoxometalates: towards advanced applications in catalysis and materials science. Chemical Communications. 2008(16):1837.
10. Chambers RC, Hill CL. Comparative study of polyoxometalates and semiconductor metal oxides as catalysts. Photochemical oxidative degradation of thioethers. Inorganic Chemistry. 1991;30(13):2776-81.
11. Hill CL. Introduction: PolyoxometalatesMulticomponent Molecular Vehicles To Probe Fundamental Issues and Practical Problems. Chemical Reviews. 1998;98(1):1-2.
12. Hiskia A, Mylonas A, Papaconstantinou E. Comparison of the photoredox properties of polyoxometallates and semiconducting particles. Chemical Society Reviews. 2001;30(1):62-9.
13. Papaconstantinou E. Photochemistry of polyoxometallates of molybdenum and tungsten and/or vanadium. Chemical Society Reviews. 1989;18:1.
14. Kormali P, Triantis T, Dimotikali D, Hiskia A, Papaconstantinou E. On the photooxidative behavior of TiO2 and PW12O403−: OH radicals versus holes. Applied Catalysis B: Environmental. 2006;68(3-4):139-46.
15. Hiskia A, Papaconstantinou E. Photocatalytic oxidation of organic compounds by polyoxometalates of molybdenum and tungsten. Catalyst regeneration by dioxygen. Inorganic Chemistry. 1992;31(2):163-7.
16. Neumann R, Levin M. Aerobic oxidative dehydrogenations catalyzed by the mixed-addenda heteropolyanion PV2Mo10O405-: a kinetic and mechanistic study. Journal of the American Chemical Society. 1992;114(18):7278-86.
17. Duncan DC, Hill CL. Mechanism of Reaction of Reduced Polyoxometalates with O2Evaluated by17O NMR. Journal of the American Chemical Society. 1997;119(1):243-4.
18. Bielski BHJ, Cabelli DE, Arudi RL, Ross AB. Reactivity of HO2/O−2 Radicals in Aqueous Solution. Journal of Physical and Chemical Reference Data. 1985;14(4):1041-100.
19. Sattari D, Hill CL. Catalytic carbon-halogen bond cleavage chemistry by redox-active polyoxometalates. Journal of the American Chemical Society. 1993;115(11):4649-57.
20. Wei Z, Wang D, Kim S, Kim SY, Hu Y, Yakes MK, et al. Nanoscale Tunable Reduction of Graphene Oxide for Graphene Electronics. Science. 2010;328(5984):1373-6.
21. Stankovich S, Dikin DA, Dommett GHB, Kohlhaas KM, Zimney EJ, Stach EA, et al. Graphene-based composite materials. Nature. 2006;442(7100):282-6.
22. Ao ZM, Hernández-Nieves AD, Peeters FM, Li S. Enhanced stability of hydrogen atoms at the graphene/graphane interface of nanoribbons. Applied Physics Letters. 2010;97(23):233109.
23. Fan Z, Yan J, Zhi L, Zhang Q, Wei T, Feng J, et al. A Three-Dimensional Carbon Nanotube/Graphene Sandwich and Its Application as Electrode in Supercapacitors. Advanced Materials. 2010;22(33):3723-8.
24. Si Y, Samulski ET. Exfoliated Graphene Separated by Platinum Nanoparticles. Chemistry of Materials. 2008;20(21):6792-7.
25. Fazaeli R, Tangestaninejad S, Aliyan H. Highly efficient conversion of aldehydes to geminal diacetates (solvent-free) and their deprotection using facile and reusable molybdenum and tungsten polyoxometalates. Applied Catalysis A: General. 2007;318:218-26.
26. Fazaeli R, Aliyan H. Clay (KSF and K10)-supported heteropoly acids: Friendly, efficient, reusable and heterogeneous catalysts for high yield synthesis of 1,5-benzodiazepine derivatives both in solution and under solvent-free conditions. Applied Catalysis A: General. 2007;331:78-83.
27. Fazaeli R, Aliyan H. A Heterogeneous catalyst for efficient and green synthesis of 2-arylbenzothiazoles and 2-arylbenzimidazoles. Applied Catalysis A: General. 2009;353(1):74-9.
28. Fazaeli R, Aliyan H, Ahmadi MA, Hashemian S. Host (aluminum incorporated mesocellulous silica foam (Al-MCF))-guest (tungsten polyoxometalate) nanocomposite material: an efficient and reusable catalyst for selective oxidation of sulfides to sulfoxides and sulfones. Catalysis Communications. 2012;29:48-52.
29. Hummers WS, Offeman RE. Preparation of Graphitic Oxide. Journal of the American Chemical Society. 1958;80(6):1339-.
30. Padmavathy N, Vijayaraghavan R. Enhanced bioactivity of ZnO nanoparticles—an antimicrobial study. Science and Technology of Advanced Materials. 2008;9(3):035004.
31. Zhang T, Zhang D, Shen M. A low-cost method for preliminary separation of reduced graphene oxide nanosheets. Materials Letters. 2009;63(23):2051-4.
32. Si Y, Samulski ET. Synthesis of Water Soluble Graphene. Nano Letters. 2008;8(6):1679-82.
33. Rauf MA, Ashraf SS. Fundamental principles and application of heterogeneous photocatalytic degradation of dyes in solution. Chemical Engineering Journal. 2009;151(1-3):10-8.
34. Djellabi R, Ghorab MF. Solar photocatalytic decolourization of Crystal violet using supported TiO2: effect of some parameters and comparative efficiency. Desalination and Water Treatment. 2013;53(13):3649-55.
35. Soutsas K, Karayannis V, Poulios I, Riga A, Ntampegliotis K, Spiliotis X, et al. Decolorization and degradation of reactive azo dyes via heterogeneous photocatalytic processes. Desalination. 2010;250(1):345-50.
36. Anandan S, Sathish Kumar P, Pugazhenthiran N, Madhavan J, Maruthamuthu P. Effect of loaded silver nanoparticles on TiO2 for photocatalytic degradation of Acid Red 88. Solar Energy Materials and Solar Cells. 2008;92(8):929-37.
37. Covarrubias C, Gracia F, Palza H. Catalytic degradation of polyethylene using nanosized ZSM-2 zeolite. Applied Catalysis A: General. 2010;384(1-2):186-91.
38. El-Mekkawi DM, Selim MM. Effect of metal loading processes on the stability and thermal transformation of Co2+- and Cu2+-zeolite Y prepared from Egyptian kaolin. Materials Characterization. 2012;69:37-44.
39. Korkuna O, Leboda R, Skubiszewska-Zie¸ba J, Vrublevs'ka T, Gun'ko VM, Ryczkowski J. Structural and physicochemical properties of natural zeolites: clinoptilolite and mordenite. Microporous and Mesoporous Materials. 2006;87(3):243-54.
40. Krissanasaeranee M, Wongkasemjit S, Cheetham AK, Eder D. Complex carbon nanotube-inorganic hybrid materials as next-generation photocatalysts. Chemical Physics Letters. 2010;496(1-3):133-8.
41. Amereh E, Afshar S. Photodegradation of acetophenone and toluene in water by nano-TiO2 powder supported on NaX zeolite. Materials Chemistry and Physics. 2010;120(2-3):356-60.
42. Kasiri MB, Aleboyeh H, Aleboyeh A. Degradation of Acid

Blue 74 using Fe-ZSM5 zeolite as a heterogeneous photo-Fenton catalyst. Applied Catalysis B: Environmental. 2008;84(1-2):9-15.
43. Barakat MA, Schaeffer H, Hayes G, Ismat-Shah S. Photocatalytic degradation of 2-chlorophenol by Co-doped TiO2 nanoparticles. Applied Catalysis B: Environmental. 2005;57(1):23-30.
44. Valkovic V, Markowicz A, Haselberger N. Review of recent applications of radioisotope excited x-ray fluorescence. X-Ray Spectrometry. 1993;22(4):199-207.
45. Saien J, Soleymani AR. Degradation and mineralization of Direct Blue 71 in a circulating upflow reactor by UV/TiO2 process and employing a new method in kinetic study. Journal of Hazardous Materials. 2007;144(1-2):506-12.
46. Zahraa O, Dorion C, Ould-Mame S, Bouchy M. Titanium dioxide deposit films for photocatalytic studies of water pollutants. Journal of Advanced Oxidation Technologies. 1999;4:40-6.
47. Sahel K, Perol N, Chermette H, Bordes C, Derriche Z, Guillard C. Photocatalytic decolorization of Remazol Black 5 (RB5) and Procion Red MX-5B—Isotherm of adsorption, kinetic of decolorization and mineralization. Applied Catalysis B: Environmental. 2007;77(1-2):100-9.
48. Tasseroul L, Pirard SL, Lambert SD, Páez CA, Poelman D, Pirard J-P, et al. Kinetic study of p-nitrophenol photodegradation with modified TiO2 xerogels. Chemical Engineering Journal. 2012;191:441-50.
49. Rao KVS, Subrahmanyam M, Boule P. Immobilized TiO2 photocatalyst during long-term use: decrease of its activity. Applied Catalysis B: Environmental. 2004;49(4):239-49.
50. Guo Y, Hu C, Jiang S, Guo C, Yang Y, Wang E. Heterogeneous photodegradation of aqueous hydroxy butanedioic acid by microporous polyoxometalates. Applied Catalysis B: Environmental. 2002;36(1):9-17.
51. Wang Y, Jing Y, Li W, Yu M, Ao X, Xie Y, et al. Silicate silver/flower-like magnalium hydroxide composites for enhanced visible light photodegradation activities. RSC Advances. 2018;8(41):23442-50.